Systematic High-Accuracy Prediction of Electron Affinities for Biological Quinones

Christine E. Schulz,[a,b,c] Achintya Kumar Dutta,[b,d] Róbert Izsák,[b,c] and Dimitrios A. Pantazis *[b,c]

Quinones play vital roles as electron carriers in fundamental biological processes; therefore, the ability to accurately predict their electron affinities is crucial for understanding their properties and function. The increasing availability of cost-effective implementations of correlated wave function methods for both closed-shell and open-shell systems offers an alternative to density functional theory approaches that have traditionally dominated the field despite their shortcomings. Here, we define a benchmark set of quinones with experimentally available electron affinities and evaluate a range of electronic structure methods, setting a target accuracy of 0.1 eV. Among wave function methods, we test various implementations of coupled cluster (CC) theory, including local pair natural orbital (LPNO) approaches to canonical and parameterized CCSD, the domain-based DLPNO approximation, and the equations-of-motion approach for electron affinities, EA-EOM-CCSD. In addition, several variants of canonical, spin-component-scaled, orbital-optimized, and explicitly correlated (F12) Møller–Plesset perturbation theory are benchmarked. Achieving systematically the target level of accuracy is challenging and a composite scheme that combines canonical CCSD(T) with large basis set LPNO-based extrapolation of correlation energy proves to be the most accurate approach. Methods that offer comparable performance are the parameterized LPNO-pCCSD, the DLPNO-CCSD(T_0), and the orbital optimized OO-SCS-MP2. Among DFT methods, viable practical alternatives are only the M06 and the double hybrids, but the latter should be employed with caution because of significant basis set sensitivity. A highly accurate yet cost-effective DLPNO-based coupled cluster approach is used to investigate the methoxy conformation effect on the electron affinities of ubiquinones found in photosynthetic bacterial reaction centers.

DOI:10.1002/jcc.25570

Introduction

Quinones are essential components of fundamental biological processes that involve electron transfer, such as photosynthesis and respiration. For example, plastoquinones are used as both intermediate and terminal electron acceptors in the oxygen-evolving photosystem II,[1–3] phylloquinone (vitamin K1) participates in electron transfer between photosystem I and ferredoxin,[4,5] and ubiquinone (coenzyme Q) is a component of electron transport chains in bacterial photosynthesis and aerobic respiration (Fig. 1).[6–8] The role of quinones as electron carriers rests on their ability to access a number of stable oxidation and protonation states, ranging from the fully oxidized to the doubly reduced and doubly protonated form, and to do so reversibly. Additionally, their electron acceptor and donor properties can be fine-tuned by varying the substituent groups on the central ring and by adjusting the properties of their immediate environment, for example through hydrogen bonding interactions in a protein pocket. It is not surprising that these features make quinones attractive also in artificial photosynthesis[9] and in technological applications such as functionalization of materials developed for energy harvesting and storage.[10–12]

Quantifying the electron accepting ability of a quinone is essential for understanding its function in any given (bio)chemical context, for gaining insight into electron transfer processes, and potentially for enabling mechanistic control. The central and fundamental property of a quinone is the electron affinity (EA). The EA determines the function of the quinone in electron transfer and also forms the basis for computing reduction potentials,[13] for which additional energetic contributions need to be considered. The computational prediction of quinone electron affinities and reduction potentials has received much attention, usually in system-specific studies.[14–27] Although approaches such as the equations-of-motion (EOM)[28] or Green's function methods provide a direct way to obtain electron affinities for multiple electron attached states in a single calculation,[28–31] quinone EAs are typically computed through differences of energies obtained by separate quantum chemical calculations of the quinone and the semiquinone radical. This places high demands on electronic structure methods because

[a] C. E. Schulz
Fakultät für Chemie und Biochemie, Ruhr-Universität Bochum, 44780, Bochum, Germany
[b] C. E. Schulz, A. Dutta, Róbert Izsák, D. A. Pantazis
Max-Planck-Institut für Chemische Energiekonversion, Stiftstr. 34-36, 45470, Mülheim an der Ruhr, Germany
[c] C. E. Schulz, Róbert Izsák, D. A. Pantazis
Max-Planck-Institut für Kohlenforschung, Kaiser-Wilhelm-Platz 1, 45470, Mülheim an der Ruhr, Germany
E-mail: dimitrios.pantazis@kofo.mpg.de
[d] A. Dutta
Department of Chemistry, Indian Institute of Technology Bombay, Mumbai 400076, India

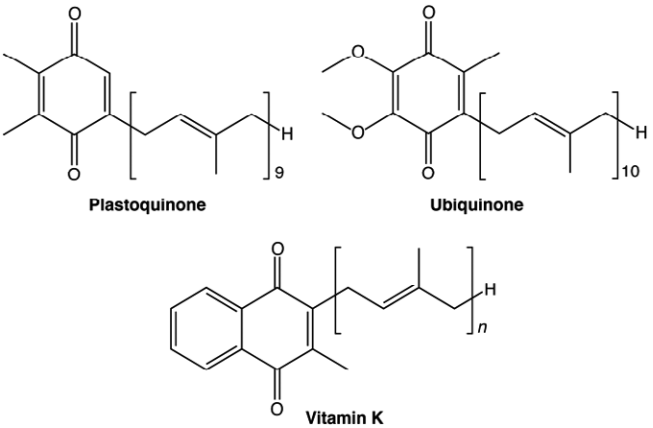

Figure 1. Representative quinones involved in biological electron transfer processes.

it requires accurate and balanced treatment of electron correlation between differently charged species that contain different numbers of paired/unpaired electrons. Existing studies typically employ density functional theory (DFT) in the form of the popular B3LYP or closely related functionals. However, a significant development in recent years has been the advent of novel computational approaches and algorithmic improvements that enable the application of correlated wave function methods to much larger systems than what would be conceivable just a few years ago, offering the promise of much higher accuracy and systematic performance for diverse chemical sets. To our knowledge, there has been so far no extensive study of modern wave function based approaches applied to the energetics of semiquinone radical formation.

Our target in the present work is to test a range of correlated wave function methods that can be applied to biologically relevant quinones, including methods that are potentially competitive with DFT in terms of computational cost[32–36] but hold the promise of systematic, consistent, and system-independent improvement in accuracy. To this end we construct a test set of 10 biologically relevant quinones with experimentally known EAs and use this set to evaluate the performance of a range of wave function and DFT methods. It is stressed that we focus exclusively on electron affinities and not on reduction potentials because we wish to isolate the contribution of the electronic structure method in the description of the quinone/semiquinone pair. In this way, we can study the general problem of minimizing intrinsic errors in the electronic structure separately from the distinct and case-dependent problem of dealing with the effect of any given chemical environment. This ensures that the conclusions are generally valid and independent from any computational approaches that may be employed for the representation and estimation of the effect of the environment, such as QM/MM treatments for proteins or various approximate models for bulk solvents.

The tested wave function methods include local pair natural orbital (LPNO)[33–35] and domain-based local pair natural orbital (DLPNO)[36,37] implementations for coupled cluster methods, the parametrized pCCSD method,[38,39] equation-of-motion coupled cluster theory (EA-EOM-CCSD),[31] as well as MP2, its spin-component-scaled variant (SCS-MP2),[40] explicitly correlated,[41] and orbital-optimized[42] implementations. Furthermore, we compare the performance of representative DFT functionals, including methods that have been proposed as more accurate than traditional hybrid functionals but have not been evaluated for the present problem.[43,44] The results allow us to define the requirements, the uncertainties, and the confidence limits of wave function and DFT approaches, and to propose a hierarchy of methods that are expected to be systematically accurate in predicting quinone electron affinities for any given size of computational problem. Finally, a study of the effect of methoxy group rotation on the electron affinity of photosynthetic bacterial ubiquinones is presented.

Methodology and Computational Details

Definition of the test set

The 10 biologically relevant 1,4-benzoquinones comprising our reference set are depicted in Figure 2. The selection was based on the basic structures of photosynthetic quinones (plastoquinone and ubiquinone), as well as on vitamin K, and the final choice of compounds was defined by the availability of experimentally determined electron affinities.[45–49] Starting from the parent para-benzoquinone, methyl substituents were added subsequently up to the tetramethyl-benzoquinone to span the range of quinones relevant to photosystem II (**1**–**6**), while 2,6-dimethoxy-parabenzoquinone (**7**) and 2,3-dimethoxy-6-methyl-paraquinone (**8**) were chosen for their relevance to the quinones of bacterial reaction centers. Finally, naphthoquinone (**9**) and 2-methyl-naphthoquinone (**10**) were added as models of vitamin K.

Geometries

For each molecule the geometries of the closed shell and the anionic species were optimized using the TPSS functional.[50] The evaluation of functionals for geometry optimizations is described in the Supporting Information and Tables S1 and S2. All calculations were done using the ORCA program package.[51] The minimally augmented[52] def2-TZVP basis sets[53] (ma-def2-TZVP) were used for optimizations. Grimme's pairwise dispersion corrections with Becke–Johnson damping (D3BJ) were applied. Coulomb fitting (RI-J) was used with decontracted universal def2/J auxiliary basis sets.[54] Increased integration grids ("Grid6" in ORCA nomenclature) and tight SCF convergence criteria were applied. Zero point energy (ZPE) corrections were determined using harmonic vibrational frequency calculations performed at the same level as the geometry optimizations.

To obtain the adiabatic electron affinity values for all methods discussed in this work, single point calculations were performed at the DFT optimized geometries. All reported adiabatic EA values include ZPE corrections (Supporting Information Table S3). In addition, single point energies of the anionic species using the neutral geometry were performed to extract vertical EAs.

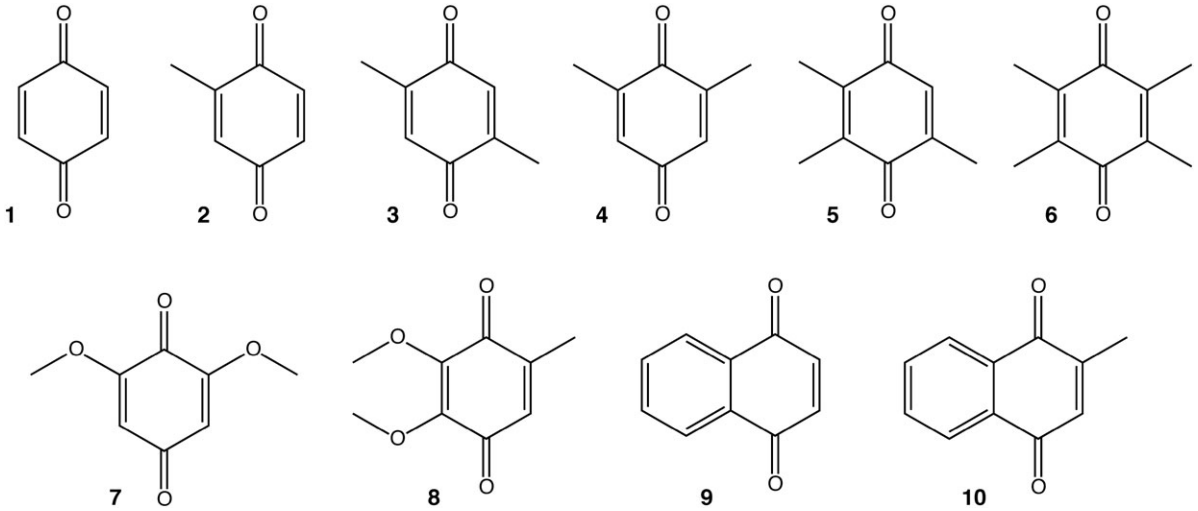

Figure 2. The quinone molecules included in the present test set.

Wave function methods

All wave function methods employed in this work make use of the aug-cc-pV*n*Z series of basis sets (n = D, T, Q). Diffuse functions (aug-) were judged to be necessary for the treatment of the anionic (semiquinone) form and to improve basis set convergence for all methods, so they were used throughout this study. In reporting results, we will be using a shorthand notation indicating only the cardinal value of the basis set, that is, "D," "T," or "Q." Two-point extrapolation for the correlation energy followed eq. (1).

$$E^{\mathrm{corr}}[X/Y] = \frac{X^{\beta}E^{(X)} - Y^{\beta}E^{(Y)}}{X^{\beta} - Y^{\beta}} \tag{1}$$

with X and Y being the cardinal numbers of each basis set indicated in brackets. In reporting basis set extrapolated results we will be using the shorthand notation [X/Y] to refer to extrapolated values, for example, [T/Q] stands for extrapolation with the aug-cc-pVTZ and aug-cc-pVQZ basis sets. If not indicated otherwise in the text, the extrapolated correlation energy is added to the HF energy obtained using the largest basis available with the same method to obtain the total extrapolated energy. The exponent β was set to 2.51 for [D/T] extrapolation and 3.05 for [T/Q] extrapolation, since these values were determined to be optimal for the aug-cc-pV*n*Z series of basis sets by Neese and Valeev.[55]

In addition to canonical coupled cluster with single and double excitations (CCSD) the parameterized coupled cluster singles and doubles approach of Huntington and Nooijen was employed (pCCSD),[38,39] in the parameterization known as pCCSD/(−1,1,1) or pCCSD/1a. The distinguishable cluster singles and doubles (DCSD) approximation by Kats et al.[56–58] is similar to pCCSD in that both approaches modify the quadratic terms in the T_2 amplitudes in the doubles residual equation of coupled cluster. Both methods perform similarly and the relation between them has been discussed in detail by Rishi et al.[59]

The local pair natural orbital (LPNO) approach was used in combination with both CCSD and pCCSD to enable the use of large basis sets reaching up to aug-cc-pVQZ. The largest extrapolation reported in the present work was achieved with the combination of aug-cc-pV[T/Q]Z basis sets. Note that perturbative triples are not implemented for LPNO-based coupled cluster methods. At the canonical CCSD(T) level the maximum basis set size that could be used for all molecules of the test set was aug-cc-pVDZ, therefore, the highest level of wave function theory reported in the present work follows a compound scheme[60] that leverages large basis set LPNO extrapolation of the CCSD correlation energy:

$$\begin{aligned} E^{\mathrm{corr}}(\mathrm{CBS}) \approx\ & E^{\mathrm{corr}}(\mathrm{LPNO\text{-}CCSD}/[\mathrm{T/Q}]) \\ & + E^{\mathrm{corr}}(\mathrm{CCSD(T)/D}) \\ & - E^{\mathrm{corr}}(\mathrm{LPNO\text{-}CCSD/D}) \end{aligned} \tag{2}$$

where D, T, and Q refer to basis sets of the aug-cc-pV*n*Z family (n = D, T, Q) as stated above.

In addition to the CBS limit, Goodson's extrapolation[61] of the coupled cluster sequence to the full CI limit was also tested. This is based on the use of a continued-fraction approximant of the form:

$$E^{\mathrm{CC,cf}} = \frac{\delta_1}{1 - \frac{\delta_2/\delta_1}{1 - \delta_3/\delta_2}} \tag{3}$$

where δ_1 is the SCF energy, δ_2 is the CCSD – SCF difference, and δ_3 is the CCSD(T) – CCSD difference.

In addition to the LPNO, the more recent domain-based DLPNO approximation was evaluated at the CCSD and CCSD(T) levels. It is noted that the perturbative triples in the implementation available to us correspond to the semi-canonical approximation (T_0). The unrestricted formalism was used in the case of the LPNO calculations for both the quinones and the semiquinones, whereas the DLPNO calculations make use of quasi-restricted orbitals (QROs), which correspond effectively to the restricted formalism for the quinones and restricted open-shell

for the semiquinones. Tight PNO criteria were used. The aug-cc-pV*n*Z/C basis sets were used as auxiliary basis sets in these calculations.[62]

The EA-EOM-CCSD method was also evaluated. The main advantage of EA-EOM-CCSD calculations is that they provide directly the vertical electron affinities as transitions from the neutral to the anion. However, the O(N^5) scaling of the iterative process and O(N^6) scaling of the ground state CCSD step, as well as the huge storage requirements of canonical EA-EOM-CCSD makes it difficult to use on the molecules included in our test set. The bt-PNO-EOM-CCSD scheme of Izsák and coworkers,[63] which involves the use of back-transformed pair natural orbitals, has lower scaling for the ground state calculation as well as for the most expensive EA-EOM term, much smaller storage requirements,[64] and gives almost identical electron affinity as that of the canonical EA-EOM-CCSD. Here, to obtain adiabatic EA values for comparison to experiment, two separate calculations need to be performed, one at the optimized geometry of the anion and the other at the optimized geometry of the neutral species. The adiabatic electron affinities are then obtained as the ground state energy at the anion geometry plus the electron affinity at the anion geometry minus the ground state energy at the geometry of the neutral. To get the basis set limit EA values in bt-PNO-EOM-CCSD, the total energy of the ground state and total energy of the anionic state (ground state energy + EA) are extrapolated separately using formula (1) and the EA values are calculated as the difference of the two extrapolated energies. The chain of spheres approximation (COSX)[65,66] was beneficially applied in the bt-PNO-EA-EOM calculations to avoid storing and manipulating the expensive four external integrals.

Other wave function methods tested include second order Møller–Plesset perturbation theory (MP2) and several variants including spin-component-scaled MP2 (SCS-MP2),[40] orbital-optimized MP2 (OO-MP2 and OO-SCS-MP2),[42] as well as explicitly correlated F12-MP2 to evaluate convergence to the complete basis set limit. The resolution of the identity (RI), also known as density fitting approximation was used in all of the above cases to speed up the calculations, in combination with the corresponding aug-cc-pV*n*Z/C auxiliary basis sets.[62] For simplicity, we will not use the "RI" label when we refer to these MP2 methods. The explicitly correlated F12-MP2 calculations made use of the cc-pVTZ-F12 basis set of Peterson et al.[67] in conjunction with appropriate complementary auxiliary basis sets (cc-pVTZ-F12-CABS).[68]

Density functional methods

In addition to the wave function methods discussed above, we tested a range of density functionals in single-point calculations, including the GGA functional PBE,[69] the meta-GGA functional TPSS,[50] the hybrid functionals B3LYP[70,71] and PBE0,[72] the hybrid meta-GGA functionals M06 and M06-2X,[73] range corrected functionals ωB97X-D3[74] and CAM-B3LYP,[75] as well as the double hybrid functionals PWPB95,[76] B2PLYP,[77] and DSD-PBEP86.[78,79] All functionals were used with D3BJ corrections, with the exception of M06 and M06-2X. The chain of spheres approximation (COSX)[65,66] was employed for Hartree–Fock exchange and the RI-MP2 approach was used for the double hybrid functionals. To evaluate the basis set influence on the DFT results, both ma-def2-TZVP and ma-def2-QZVPP basis sets were used, with decontracted auxiliary def2/J basis sets. All DFT electron affinities reported in the main text are obtained with the ma-def2-QZVPP basis sets and include the same ZPE corrections applied to the wave function methods. Increased integration accuracy ("Grid6" and "GridX9" in ORCA nomenclature) and tight SCF convergence criteria were used throughout.

While in this study we have restricted our attention to widely available efficient DFT functionals, we note in passing that promising functionals have also been developed within the framework of reduced density matrix functional theory. One may single out the Piris natural orbital functionals[80,81] as an example and interested readers are referred to a recent review[82] discussing many other approaches and advances. In particular, some of these functionals have also been tested for the evaluation of ionization potentials and electron affinities.[83,84]

Target accuracy

A question that needs to be addressed before discussing the results of the present study concerns the desired level of accuracy in the prediction of quinone electron affinities. This decision is to some extent arbitrary, or at least case-dependent, and will be influenced in practice by the actual performance of the available computational methods. Nevertheless, given that our focus is on biologically relevant quinones, we suggest that one may arrive at a plausible value for a protein setting by inspecting some data from a biological system. We use as example the case of photosystem II (Fig. 3). There, the electron affinities of the primary and secondary acceptor plastoquinones Q_A and Q_B,

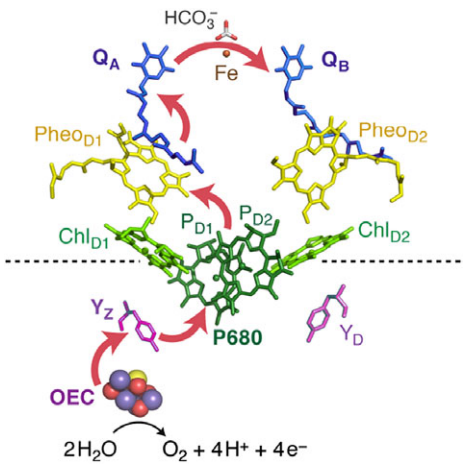

Figure 3. Redox active cofactors involved in electron transfer in photosystem II, which transfers electrons from water to a plastoquinone Q_B, oxidizing the former to dioxygen. The horizontal dashed line through the site of light-induced charge separation P680 separates the "donor side" from the "acceptor side" of the enzyme. Red arrows indicate the flow of electrons from water to the reaction center chlorophyll assembly P680 and from the reaction center to the primary (Q_A) and terminal acceptor Q_B. [Color figure can be viewed at wileyonlinelibrary.com]

Table 1. Calculated adiabatic electron affinities (eV) for the 10 quinones of the reference set, obtained with coupled cluster methods and selected basis sets and basis set extrapolation combinations

	1	2	3	4	5	6	7	8	9	10	MSE	MAX	RMS
CCSD/[D]	1.68	1.61	1.55	1.55	1.49	1.46	1.51	1.70	1.59	1.52	−0.21	−0.24	0.21
CCSD(T)/[D]	1.77	1.71	1.64	1.65	1.60	1.56	1.60	1.76	1.69	1.63	−0.11	−0.14	0.12
bt-PNO-EOM-CCSD/[T/Q]	1.79	1.70	1.63	1.64	1.56	1.50	1.55	1.73	1.67	1.57	−0.14	−0.17	0.14
LPNO-CCSD/[D/T]	1.80	1.73	1.66	1.67	1.61	1.59	1.60	1.79	1.68	1.54	−0.11	−0.20	0.11
LPNO-CCSD/[T/Q]	1.79	1.72	1.65	1.65	1.59	1.55	1.58	1.77	1.67	1.61	−0.12	−0.14	0.12
DLPNO-CCSD/[D/T]	1.76	1.68	1.61	1.61	1.55	1.52	1.53	1.72	1.64	1.63	−0.15	−0.19	0.15
DLPNO-CCSD/[T/Q]	1.74	1.66	1.59	1.59	1.53	1.49	1.51	1.69	1.62	1.52	−0.18	−0.22	0.18
LPNO-pCCSD/[D/T]	1.82	1.74	1.68	1.68	1.63	1.60	1.63	1.80	1.70	1.60	−0.08	−0.14	0.09
LPNO-pCCSD/[T/Q]	1.83	1.75	1.68	1.69	1.63	1.59	1.62	1.81	1.73	1.63	−0.08	−0.11	0.08
DLPNO-CCSD(T_0)/[D/T]	1.86	1.79	1.71	1.71	1.66	1.61	1.61	1.78	1.74	1.74	−0.05	−0.11	0.06
DLPNO-CCSD(T_0)/[T/Q]	1.83	1.76	1.68	1.68	1.63	1.58	1.58	1.75	1.71	1.61	−0.09	−0.14	0.10
CCSD(T)/[D] + $E^{CC,cf}$	1.78	1.72	1.66	1.66	1.61	1.57	1.61	1.77	1.70	1.64	−0.10	−0.13	0.10
DLPNO-CCSD(T_0)/[Q] + $E^{CC,cf}$	1.83	1.76	1.68	1.68	1.63	1.58	1.57	1.74	1.71	1.62	−0.09	−0.15	0.10
CCSD(T) + E^{corr}/CBS	1.87	1.81	1.74	1.75	1.70	1.65	1.69	1.84	1.79	1.76	−0.01	−0.04	0.03
Experiment	1.91	1.85	1.76	1.77	1.69	1.62	1.72	1.86	1.81	1.74			

Mean signed errors (MSE), maximum signed errors (MAX), and root mean squared errors (RMS) in eV are given against the experimental values.

the factors that control them, and the sequence of reduction and protonation of Q_B are questions with critical implications for biological photosynthesis,[2,85] and remain open challenges for both experiment and theory.[86–99]

The midpoint potential of the primary plastoquinone acceptor Q_A is uncertain because a wide scatter of values have been assigned experimentally, nevertheless the quinone is suggested to be present in two forms that differ by 0.12–0.15 V, while the difference in potential between the primary acceptor Q_A and the terminal acceptor Q_B is estimated at approximately 0.19 V.[88,92,98,100,101] Small changes in hydrogen bonding and in long-range interactions are known to cause shifts up to 0.10 V, while treatment with common herbicides is known to induce shifts in the Q_A potential of the order of 0.05 V. Structural or chemical perturbations at metal binding sites of the enzyme cause midpoint potential shifts of 0.02–0.04 V, which are critical for determining the lifetimes of intermediates and regulating the kinetics of electron transfer.[85,102,103] From the above cursory exposition of literature values it appears that for reliable computational studies a useful target accuracy for quinone electron affinities in absolute terms should be better than 0.1 eV in general, and systematically better than that for truly predictive work.

Table 2. Basis set dependence of various coupled cluster implementations

	MSE	MAX	RMS
CCSD/D	−0.19	−0.24	0.20
CCSD(T)/D	−0.10	−0.13	0.10
LPNO-CCSD/D	−0.20	−0.30	0.21
LPNO-CCSD/T	−0.15	−0.20	0.15
LPNO-CCSD/Q	−0.13	−0.18	0.13
LPNO-CCSD/[D/T]	−0.09	−0.22	0.10
LPNO-CCSD/[T/Q]	−0.10	−0.16	0.11
DLPNO-CCSD/D	−0.23	−0.29	0.23
DLPNO-CCSD/T	−0.19	−0.27	0.20
DLPNO-CCSD/Q	−0.18	−0.26	0.19
DLPNO-CCSD/[D/T]	−0.13	−0.16	0.14
DLPNO-CCSD/[T/Q]	−0.17	−0.25	0.17
LPNO-pCCSD/D	−0.17	−0.25	0.17
LPNO-pCCSD/T	−0.11	−0.19	0.12
LPNO-pCCSD/Q	−0.09	−0.16	0.09
LPNO-pCCSD/[D/T]	−0.07	−0.16	0.08
LPNO-pCCSD/[T/Q]	−0.06	−0.13	0.07
DLPNO-CCSD(T_0)/D	−0.18	−0.26	0.18
DLPNO-CCSD(T_0)/T	−0.11	−0.17	0.11
DLPNO-CCSD(T_0)/Q	−0.09	−0.16	0.10
DLPNO-CCSD(T_0)/[D/T]	−0.04	−0.08	0.04
DLPNO-CCSD(T_0)/[T/Q]	−0.08	−0.15	0.08

Mean signed errors (MSE), maximum signer errors (MAX), and root mean squared errors (RMS) in eV for electron affinities referenced against the extrapolated CCSD(T) values.

Results and Discussion

Coupled cluster methods

A summary of the adiabatic electron affinities obtained in this study with coupled cluster methods in various implementations is given in Table 1 (see Supporting Information Table S4 for vertical electron affinities). The results in general show a small but systematic underestimation of EA values. Qualitatively, all methods reproduce the decrease in EA across the subset of quinones **1**–**6**, with the highest EA predicted for para-benzoquinone **1**, the lowest EA for the fully substituted tetramethyl derivative **6**, and the isomeric quinones **3** and **4** being practically equivalent in terms of EA. An interesting observation is that although the numerical values differ between methods, they all predict quinone **7** to have the lowest EA of the test set. This is a point we will return to in the following. The worst method on average is CCSD combined with the smallest basis set used in this work, aug-cc-pVDZ. However, to place the absolute values in perspective, the error of this "worst case" method is already an order of magnitude better than the Hartree–Fock electron affinities, which have a mean signed error of −1.25 eV. At the opposite end is the composite method described in the Methodology section, which combines canonical CCSD(T)/D with LPNO-CCSD/[T/Q] extrapolation. This method shows the lowest errors compared to experiment among all other coupled cluster approaches, and indeed with mean signed and root-

mean-squared (RMS) errors of −0.021 eV and 0.045 eV it is the best method tested in the present work. In this sense, it can be used to benchmark more approximate methods in cases where experimental reference electron affinities are not available.

The basis set dependence of various methods is explored with more detail in Table 2, where it is shown that all coupled cluster approaches form a more or less regular progression that converges toward the most accurate method employed, the composite extrapolated CCSD(T). With one exception that will be discussed below, for all methods where the full sequence of aug-cc-pV*n*Z (*n* = D, T, Q) basis sets can be applied, the decrease in error generally follows the sequence D > T > Q > [D/T] > [T/Q]. It is important to note the superior accuracy of the [D/T] extrapolation over the quadruple-ζ results in most cases. In anticipation of the results obtained with other methods (both MP2 and DFT) that will be presented in subsequent sections of this work, it is stressed that the direct use of non-extrapolated coupled cluster energies obtained with a single basis set should be avoided. This is especially so in the case of the double-ζ basis because the errors are comparable or larger than those obtained with much cheaper methods such as mainstream density functionals, hence negating the relevance of coupled cluster approaches.

The results of Table 1 and the sequence presented in Table 2 allow us to gain some insight into the physics of the problem and to better define the energetic contributions that determine the accuracy of each approach. First of all, the canonical CCSD errors are reduced approximately by half on inclusion of perturbative triples, using the same aug-cc-pVDZ basis set. The LPNO-CCSD shows negligible deviations from the reference method compared to canonical CCSD with the same basis set. Therefore, the error in canonical CCSD arising from the use of a small basis is much larger than the truncation error in LPNO-CCSD[33,34] and the extrapolated LPNO-CCSD values with larger basis sets are expected to reliably reflect the basis set convergence behavior of CCSD. In this respect, it is important to note that the reduction of average errors in EA values on inclusion of perturbative triples (i.e., CCSD/D versus CCSD(T)/D) and the reduction in errors on large-basis extrapolation (LPNO-CCSD/[T/Q]) are of similar magnitude and direction. Therefore, it can be concluded that the accurate calculation of quinone electron affinities with coupled cluster methods depends almost equally on the basis set incompleteness error and the treatment of the triples excitations. In other words, the errors from basis set incompleteness and from the missing (T) are additive, and hence, it is precisely the minimization of both errors in the composite method, via inclusion of (T) at the moderate basis set and the CCSD extrapolation using the LPNO implementation with large basis sets, that results in the remarkably favorable performance of the compound approach. Conversely, dealing with only one of these sources of error is insufficient to reduce the average errors below the 0.1 eV mark.

The LPNO approach approximates the canonical method in the sense that it will reproduce the canonical results with sufficiently tight thresholds, while the DLPNO method introduces the further approximation of partitioning into orbital domains. Table 2 allows comparison of the average EA errors by the LPNO and DLPNO approximations to the errors of canonical CCSD with the same sequence of basis sets. It can be seen that the basis set convergence behavior is slightly different, because the DLPNO-CCSD results with the aug-cc-pVTZ basis set are already well converged and show limited improvement on further increasing the basis set. This is also reflected in the extrapolated values, as for DLPNO the [D/T] extrapolation already yields EAs that are not improved with the more demanding [T/Q] extrapolation. This does not hold exactly for the vertical electron affinities compared to the reference method (Supporting Information Table S5), where the mean average error with the [T/Q] extrapolation is marginally better.

It is interesting to look a bit closer at the apparent differences between the LPNO and DLPNO approach at the CCSD level, since the latter seem to be associated with larger average errors compared to the former. Comparison of the absolute correlation energies produced by the various approaches with the aug-cc-pVDZ basis set against the canonical CCSD (Supporting Information Table S6) confirms that the DLPNO-CCSD reproduces the canonical results much more closely in absolute terms. Specifically, DLPNO-CCSD recovers 99.98% of the canonical CCSD correlation energy for the neutral species and 99.80% for the anions, versus 99.49% and 99.46% of LPNO. In absolute terms, LPNO underestimates the correlation energy by a mean value of 140 meV for the neutral and 147 meV for the anions, whereas DLPNO achieves superior recovery with underestimations of merely 6 meV and 53 meV. But these values also suggest that although the DLPNO approach is clearly superior to LPNO, it is not *equally* superior for *both* the closed and the open-shell system. Hence, the LPNO approach at the CCSD level benefits from error cancellation when total energy differences are computed, with the result that on average it deviates by 9 meV in final electron affinities from the canonical CCSD/D values compared to the DLPNO deviation of 32 meV. It might be useful to investigate the relevant technical points further to understand where the slight imbalance in correlation energy for the DLPNO treatment of the closed-shell versus the open-shell case originates from. However, we will not branch into this type of investigation here. For the present purposes, and for future applications, we favor the use of the DLPNO approach for two simple reasons: first, the tremendous advantage of the linear-scaling DLPNO-CCSD implementation allows it to be applied to exceedingly large systems, and second, the ability to address the effect of the triples excitations, currently only possible with the DLPNO approach, is an overwhelming and decisive factor for achieving high accuracy in practice.

Before discussing methods that attempt to consider the effect of the triples corrections to the correlation energy, we would like to discuss briefly the performance of the bt-PNO-EOM-CCSD approach. From Table 1 it is clear that in comparison to experiment the method performs similarly to DLPNO-CCSD (with [D/T] extrapolation) and worse than LPNO-CCSD. It should be noted however that the error obtained in bt-PNO-EOM-CCSD is below the error bar of the EOM-CCSD method itself.[104] Since the effect of triples is also missing from the presently used bt-PNO-EOM-CCSD scheme, it is expected

that their inclusion in a future EOM implementation would significantly improve the accuracy of the predicted EAs. This would be an important development because in addition to the improved accuracy it would enable one to enjoy at the same time the substantial benefits of the EOM approach with a much smaller computational cost than that of CCSD(T).[105] Moreover, if one considers cases that involve doubly reduced species (an example is the terminal plastoquinone Q_B of photosystem II that may be reduced twice prior to protonation) the EOM approach would have a substantial advantage over other methods that might struggle to describe the dianion and would require multiple well-converged calculations on three differently charged species.[106] Conversely, we would like to note that inclusion of triples may not be a universal requirement in the EOM-CC calculation of ionization potentials and electron affinities, because good results have been reported for other systems, for example, DNA and RNA nucleobases.[107–110] Regardless of the potential of the method, with the present implementation it cannot be considered competitive to the best alternative coupled cluster approaches tested in this work.

As noted above, the triples corrections are an essential factor for improving the accuracy of electron affinities. The available LPNO implementations do not cover triples corrections, so the approach cannot be extended beyond CCSD. The pCCSD method of Huntington and Nooijen attempts to compensate for the missing triples through parametrization.[38] Indeed this seems to be partially successful, because LPNO-pCCSD consistently outperforms LPNO-CCSD by approximately the same margin of 0.03–0.04 eV at each basis set increment. Thus, the combination of LPNO-enabled use of large basis sets and the parametric inclusion of the effect of the triples excitations results in LPNO-pCCSD achieving average errors in electron affinities below the 0.1 eV target accuracy. Indeed, the use of LPNO-pCCSD with [D/T] extrapolation is a cost-effective option that offers improved performance without explicitly considering some form of perturbative triples. It is expected that similar methods such as the distinguishable cluster approach would perform comparably well.

The DLPNO approach currently allows computation of the semi-canonical triples (T_0), a noniterative correction that ignores the couplings between different triples by the off-diagonal Fock matrix elements. The results obtained in this way, labeled as DLPNO-CCSD(T_0) in Tables 1 and 2, represent a remarkable improvement over the DLPNO-CCSD values at equivalent basis sets. The DLPNO-CCSD(T_0) results with the [D/T] extrapolation are in fact the second-best in terms of agreement with experimental electron affinities (Table 1), and represent the best approximation to the composite reference method (Table 2). The [T/Q] extrapolation does not yield consistently a further improvement. It can be expected that future developments in advancing the DLPNO-based treatment of triples corrections beyond the semi-canonical approximation[111] will further improve the performance of the method.

Comparing the continued-fraction extrapolation with the CBS extrapolation, a small improvement on addition of $E^{CC,cf}$ is observed for non-extrapolated methods in combination with small basis sets like CCSD(T)/[D] (Table 1). For larger basis sets, the addition of $E^{CC,cf}$ to DLPNO-CCSD(T_0)/[Q] does not yield an improvement compared to the CBS extrapolated DLPNO-CCSD (T_0)/[T/Q] values. In addition, it should be noted that the Goodson extrapolation is applicable to methods with perturbative triples (or higher) corrections, which is currently not the case for, for example, LPNO-pCCSD. Therefore, CBS extrapolation appears to offer a less method-dependent and more effective way of obtaining improved results, at least for the present systems and property of interest.

In conclusion, the most accurate coupled cluster approach employed in this work is a composite method that combines canonical CCSD(T) energies obtained at a moderately sized aug-cc-pVDZ basis set with LPNO-CCSD extrapolation energies at higher cardinal numbers. This leads to the best possible error control; in fact, the maximum absolute error of the method would be merely 0.04 eV if it were not for quinone **7**. The problematic performance for this molecule may suggest that it is worth revisiting the experimental assignment. More approximate methods include the parametrized LPNO-pCCSD and the DLPNO-CCSD(T_0), both of which are recommended to be used with aug-cc-pV[D/T]Z extrapolation since the use of higher cardinal numbers does not justify the increased cost.

Table 3. Calculated adiabatic electron affinities (eV) for the 10 quinones of the reference set, obtained with MP2 methods

	1	2	3	4	5	6	7	8	9	10	MSE	MAX	RMS
MP2/D	1.78	1.70	1.66	1.60	1.58	1.58	1.27	1.59	1.66	1.55	−0.18	−0.45	0.21
MP2/T	1.84	1.75	1.71	1.64	1.62	1.63	1.27	1.60	1.71	1.64	−0.13	−0.45	0.18
MP2/Q	1.86	1.76	1.73	1.66	1.64	1.65	1.28	1.60	1.73	1.66	−0.12	−0.44	0.17
MP2/[D/T]	1.89	1.79	1.76	1.69	1.66	1.68	1.31	1.63	1.77	1.73	−0.08	−0.41	0.15
MP2/[T/Q]	1.88	1.78	1.75	1.67	1.65	1.67	1.29	1.62	1.75	1.68	−0.10	−0.43	0.16
MP2-F12	1.87	1.78	1.75	1.68	1.66	1.67	1.31	1.62	1.75	1.67	−0.10	−0.41	0.16
SCS-MP2/T	1.56	1.47	1.44	1.37	1.35	1.37	1.06	1.36	1.47	1.37	−0.39	−0.66	0.41
SCS-MP2/Q	1.58	1.49	1.46	1.39	1.36	1.38	1.07	1.36	1.49	1.38	−0.38	−0.65	0.39
SCS-MP2/[T/Q]	1.60	1.51	1.48	1.40	1.38	1.40	1.08	1.36	1.51	1.40	−0.36	−0.64	0.38
OO-MP2/T	2.03	1.96	1.89	1.90	1.85	1.79	1.65	1.87	1.94	1.87	0.06	−0.45	0.19
OO-MP2/Q	2.07	1.99	1.92	1.92	1.87	1.81	1.68	1.88	1.97	1.90	0.09	−0.44	0.20
OO-SCS-MP2/T	1.80	1.74	1.67	1.68	1.63	1.58	1.44	1.71	1.74	1.67	−0.11	−0.28	0.13
OO-SCS-MP2/Q	1.84	1.77	1.70	1.71	1.65	1.60	1.47	1.72	1.77	1.70	−0.08	−0.25	0.10
Experiment	1.91	1.85	1.76	1.77	1.69	1.62	1.72	1.86	1.81	1.74			

Mean signed errors (MSE), maximum signed errors (MAX), and root mean squared errors (RMS) in eV are given against the experimental values.

MP2 methods

In the present section we examine the MP2 method and a few of its variants. The methods presented in Table 3 (for vertical EAs see Supporting Information Table S7) show weaker dependence on basis set size compared to the coupled cluster approaches discussed above, and hence it is easier to reach the basis set limit of each method. This is confirmed by the explicitly correlated F12-MP2 results, which are practically indistinguishable from the MP2/[T/Q] extrapolated values. Nevertheless, the electron affinities computed with the individual basis sets, particularly for the triple-ζ basis, have non-negligible differences from the converged results; therefore, extrapolation is still advised for MP2 methods. An important conclusion from Table 3 is that MP2 performs quite well, meeting the target accuracy of better than 0.1 eV in the mean signed error for electron affinities. Conversely, it exhibits a wider spread of errors compared to the best performing coupled cluster methods of Table 1. A remarkable observation is that the spin-component-scaled variant SCS-MP2 fares particularly badly for quinone electron affinities and is in fact the worst method encountered so far in this work. In the SCS approach separate weights are used for opposite-spin and same-spin contributions to the correlation energy (1.2 and 0.333 following Grimme).[40] SCS-MP2 is known to correct some shortcomings of conventional MP2 in various applications, but this is clearly not the case here.

Orbital optimized methods not only minimize the MP2 energy with respect to the MP2 amplitudes, but additionally minimize the total energy with respect to changes in the orbitals, making the Hylleraas functional stationary with respect to orbital rotations. Both OO-MP2 and OO-SCS-MP2 methods were tested here. Note that because the orbitals are changed to minimize the total energy in OO methods, the standard basis set extrapolation formula is not applicable. From the results of Table 3 it appears that orbital optimization in the case of MP2 is not clearly beneficial for the specific problem. In particular, it does not improve the average errors, but it inverts the systematic underestimation of experimental EAs by MP2 to an overestimation by a similar magnitude. Where orbital optimization has a significant effect is instead on the SCS-MP2 variant. The OO-SCS-MP2 method completely corrects the problematic behavior of SCS-MP2 and, in combination with the largest aug-cc-pVQZ basis set, leads to the best performing method in Table 3. This, however, comes at a great computational cost, which for OO methods is approximately an order of magnitude greater than RI-(SCS)-MP2.

The above results allow us to conclude that classical MP2 or orbital optimized OO-SCS-MP2 might be dependable choices for predicting quinone electron affinities if basis set convergence is ensured. However, they are not necessarily more cost effective (this is especially not the case for the costly orbital-optimized methods) and certainly do not match the systematic accuracy and tight error control of the LPNO or DLPNO coupled cluster methods discussed in the previous section, therefore, it is hard to advocate their use in practical applications.

DFT methods

In view of the dominant use of density functional methods in the area of quinone electron affinities and reduction potentials, particularly in biomolecules, it is necessary to investigate how common functionals compare against the wave function methods presented above. Table 4 summarizes the electron affinities and error statistics for a number of DFT methods covering various functional classes. We note that Minnesota functionals, range-corrected functionals, and double-hybrid functionals have not been systematically benchmarked before for the present problem. For all molecules in our test set, the spin density of the semiquinone radical anion is delocalized over the ring, with prominent contributions of the two oxygen atoms (see Supporting Information Fig. S1 for spin density plots of all anions obtained from M06 calculations). There is practically no variation in spin expectation values among the 10 quinones for a given functional, and little variation among different functionals (Supporting Information Table S8), other than a tendency toward higher values with increased exact exchange, and for double hybrid functionals. The spin distribution as judged by Mulliken spin populations is similar across functionals, with the double hybrids favoring a slightly increased localization of spin on the oxygen atoms versus the

Table 4. Calculated adiabatic electron affinities (eV) for the 10 quinones of the reference set, obtained using different DFT functionals with the ma-def2-QZVPP basis set

	1	2	3	4	5	6	7	8	9	10	MSE	MAX	RMS
PBE	2.20	2.10	2.01	2.02	1.96	1.88	1.79	1.94	2.09	1.99	0.22	0.29	0.24
TPSS	2.12	2.03	1.94	1.95	1.89	1.82	1.75	1.86	2.00	1.91	0.15	0.21	0.17
PBE0	2.16	2.06	1.96	1.97	1.91	1.84	1.80	1.97	2.02	1.93	0.19	0.25	0.20
B3LYP	2.09	1.99	1.90	1.91	1.84	1.77	1.78	1.90	1.94	1.85	0.12	0.18	0.13
M06	2.01	1.93	1.84	1.86	1.80	1.74	1.66	1.88	1.89	1.80	0.07	0.12	0.08
M06-2X	2.13	2.04	1.95	1.96	1.90	1.84	1.84	2.03	2.00	1.91	0.19	0.22	0.19
ωB97X-D3	2.05	1.96	1.87	1.88	1.82	1.76	1.75	1.94	1.90	1.81	0.10	0.14	0.11
CAM-B3LYP	2.15	2.06	1.96	1.97	1.90	1.84	1.87	2.02	1.99	1.90	0.19	0.24	0.19
PWPB95	1.87	1.79	1.71	1.71	1.66	1.61	1.56	1.73	1.76	1.68	−0.07	−0.16	0.08
B2PLYP	1.97	1.88	1.80	1.81	1.75	1.69	1.66	1.82	1.84	1.76	0.03	0.07	0.05
DSD-PBEP86	1.88	1.80	1.73	1.73	1.67	1.63	1.58	1.76	1.77	1.69	−0.05	−0.14	0.06
Experiment	1.91	1.85	1.76	1.77	1.69	1.62	1.72	1.86	1.81	1.74			

Mean signed errors (MSE), maximum signed errors (MAX), and root mean squared errors (RMS), in eV, compared with the experimental values.

ipso carbons (see Supporting Information Table S9 for a comparison of spin populations for semiquinone **1**).

The results listed in Table 4 indicate that DFT methods yield mixed results. Most functionals tend to overestimate electron affinities, something also observed for other systems in the past.[112] Among the different electronic structure situations that can arise in relation to an EA calculation, Curtiss et al.[113] had identified the case of closed-shell neutral to open-shell anion as the most problematic for DFT methods. The present quinone test set falls in this category, for which the large average errors were attributed to overestimation of the stability of the open-shell anion and related to the fact that the HOMO of the anion is not occupied in the neutral—as opposed to, for example, the situation where an open-shell neutral form is reduced to a closed-shell anion.[112] A pertinent methodological point[114–120] that relates to the applicability of DFT for electron affinities[112,121,122] relates to the observation that the increased self-interaction error when DFT is applied to anions can artificially raise the energy of Kohn–Sham orbitals, potentially leading to positive orbital eigenvalues. It has been argued that in this case meaningful electron affinities from DFT may actually be the result of the opposing error introduced by the finite basis, which stabilizes states that might otherwise be unbound. In the present set of compounds, we observe that positive eigenvalues for the highest occupied Kohn–Sham orbitals can occur for anions with the PBE0 and TPSS functionals when the largest applicable basis sets are used. However, in all other cases the highest occupied orbitals of all semiquinones have negative eigenvalues.

The GGA functional PBE appears to yield the least accurate results compared to the reference method, with a mean signed error of 0.23 eV and a maximum error of 0.29 eV (for quinone **1**). The corresponding hybrid PBE0 shows a smaller mean signed error, but still performs worse than the popular functionals TPSS and B3LYP. The best performing hybrid is the Minnesota functional M06 (27% exact exchange) with a mean signed error of 0.07 eV and a maximum absolute error of 0.12 eV (for quinone **6**) compared to experiment. It also has the narrowest spread of errors (0.14 eV) compared to all other functionals, that is, the errors are more systematic. With the exception of the double hybrids, M06 is the only functional that achieves MAE and RMS values lower than 0.1 eV. Conversely, M06-2X, which has double the amount of Hartree–Fock exchange compared to M06, shows inferior performance, similar to PBE0 and no better than TPSS. This is an important observation because a recent benchmark study of ionization energies highlighted M06-2X (with 54% exact exchange) as the best performing functional by far, surpassing double hybrid functionals and outperforming M06 by more than a factor of two in the mean unsigned error.[123] The reverse situation is witnessed in the present results, suggesting that the two functionals perform differently for different processes and chemical systems, presumably at least in part because the percentage of Hartree–Fock exchange cannot be tuned in a universal manner. Therefore, although Minnesota functionals often rise to the top ranks of various benchmarks and applications, a careful selection is still required between different variants on a case-by-case basis. It would be interesting to see whether a new generation of functionals perform even better than M06, given that MN15 has been reported to improve on electron affinities of the EA13 reference set.[124]

Recent findings in the literature suggest that long-range corrected functionals are appropriate for the calculation of EA values,[125] so we tested two such functionals, ωB97X-D3 and CAM-B3LYP. The former performs quite well, although not on a par with M06, but CAM-B3LYP represents a deterioration across the board compared to B3LYP. Therefore, there is no clear benefit from this class of functionals in the calculation of quinone electron affinities.

The best performing subset of functionals for the present test set are the double hybrids, with B2PLYP achieving the smallest average, maximum, and RMS errors, followed by DSD-PBEP86 and PWPB95. An aspect that differentiates the behavior of the latter two compared to other functionals is that they slightly underestimate electron affinities, analogously to most wave function methods.

The amount of HF exchange for the hybrid and double hybrid functionals may partly influence the quality of results, but no systematic correlation can be identified. Double hybrid functionals cover the large percentage range, ranging from 50% (PWPB95) to almost 70% (DSD-PBEP86). B2PLYP, which yields the best results, contains 53% HF exchange. Among the hybrid functionals M06 (27% HF exchange) shows better agreement to experiment than M06-2X (54% HF exchange), while PBE0, which has a similar amount of HF exchange as M06 (25%), shows poorer performance than even the nonhybrid TPSS. It is clear, therefore, that the percentage of Hartree–Fock exchange is not a decisive determinant of DFT performance for the present property.

An important methodological point relates to the convergence of electron affinities with respect to the size of the basis set. Results obtained with the ma-def2-QZVPP basis sets are reported for all DFT methods, but most functionals yield converged results already with the ma-def2-TZVP basis sets, although M06 and ωB97X-D3 show somewhat higher sensitivity than other functionals in their families (shifts of the order of 0.02 eV and 0.01 eV, respectively). In contrast, double hybrid functionals are not yet converged with the ma-def2-TZVP basis set and large changes are seen on increase to ma-def2-QZVPP (see Supporting Information Table S10). B2PLYP is the most sensitive functional, displaying shifts of up to 0.1 eV in adiabatic EA values from the triple-ζ to the quadruple-ζ basis, followed by PWPB95. Such large shifts can directly affect the mean errors associated with the method: the MSE for PWPB95 changes from −0.14 eV to −0.07 eV while that of B2PLYP even changes sign, from −0.06 eV to 0.02 eV. Similar observations regarding the increased demands of double hybrid functionals on basis set size are known from other studies,[43,76] but the changes witnessed here are rather large with respect to the absolute value of the quantity of interest, and hence some uncertainty remains as to whether the double hybrid electron affinities are fully converged. This has implications for practical applications and suggests that the behavior of double hybrids must be carefully

evaluated with respect to basis set dependence and their ability to produce converged electron affinities.

Presumably this large basis set dependence is related to the MP2 component of the method, so it would be interesting to evaluate approaches that can address this problem in an efficient and computationally robust manner, either converging toward complete basis set results,[126,127] or using orbital-optimized approaches,[128,129] or even applying correlation methods that go beyond MP2.[130] There are interesting recent developments in all these areas with respect to improvements in double hybrid functionals. Although we do not intend to pursue such avenues in the present work, we have tested the possibility of obtaining converged results for B2PLYP by substituting the MP2 part with explicitly correlated MP2-F12 (using cc-pVTZ-F12 basis sets for both the Kohn–Sham and the MP2-F12 part). This variant shows significantly deteriorated accuracy, with a mean signed error that is 10 times worse than the standard B2PLYP results (0.233 eV vs. 0.021 eV). This might be an indication that B2PLYP benefits partially from basis set related error cancellation, but further analysis is necessary in this direction before safe conclusions can be reached.

Overall, the use of a double hybrid functional with a basis set at least as large as ma-def2-QZVPP can yield highly accurate quinone electron affinities. Depending on the level of accuracy required, the cheaper GGA and hybrid functionals can be considered appropriate for semi-quantitative purposes in view of their minimal cost compared to correlated wave function methods. Still, there is good reason to prefer the wave function alternatives discussed in the previous sections where possible because of the expected consistency across different systems and for different properties, including cases where double hybrids may show variable performance.[123,131,132]

Application to ubiquinone 2-methoxy rotation

Bacterial reaction centers employ two ubiquinones, UQ_A and UQ_B, as intermediate and terminal electron acceptors, similar to the plastoquinone sites in the acceptor side of photosystem II (Fig. 3).[1,133] A defining property of the system is that the two chemically identical ubiquinone molecules have a difference in reduction potentials of about 60–75 mV enabling forward electron transfer.[134–136] This difference may be the result of a significant electrostatic effect of the protein environment, as in the case of the plastoquinones of photosystem II. Indeed, it was reported that a classical electrostatics simulation can fully account for the higher potential of UQ_B.[137] However, the presence of the methoxy groups in the ubiquinones provides an additional means for modulation of their electron affinity.[27,138–144] This can be effected through the balance between the electron withdrawing effect when the methoxy group is out of the ring plane and the electron donating effect due to conjugation when the methoxy group is in-plane. IR difference spectra of anion/neutral pairs for UQ_A and UQ_B showed no evidence for conformational inequivalence between the two sites,[145] but recent analysis of ^{13}C hyperfine coupling constants from hyperfine sublevel correlation (HYSCORE) studies with ^{13}C labeled quinones clearly demonstrated that the 2-methoxy group (the one at *meta*-position with respect to the polyisoprenyl chain, Fig. 4) adopts distinct conformations between UQ_A and UQ_B.[142] Moreover, reconstitution studies with synthetic quinones in *Rhodobacter sphaeroides* established that the 2-methoxy group is required for electron flow between the two sites,[146] consistent with the hypothesis that the 2-methoxy conformation plays a direct role in modulating the electron affinity of the ubiquinones.

A question that arises naturally is what are the relative contributions of nonspecific protein effects versus the modulation of the electron affinity through 2-methoxy rotation? Quantifying the electrostatic effect of the protein on each site quantum mechanically is complicated both methodologically and by the lack of highly resolved and conformationally unique structures for the binding pockets. By contrast, the effect of the 2-methoxy conformation on the electron affinity can be precisely probed and quantified using computational studies on independent ubiquinone models. In the following we quantify this effect using the most accurate applicable level of coupled cluster theory identified in this work to produce reference values for the ubiquinone system. Even with the aug-cc-pVDZ basis set, canonical CCSD(T) results are here challenging or impossible to complete. This, however, poses no limitation for the DLPNO-CCSD(T_0) approach, which we apply here with the optimally performing (Tables 1 and 2) aug-cc-pV[D/T]Z extrapolation. To our knowledge, this is the first attempt to apply highly accurate wave function methods to this crucial biophysical problem.

A ubiquinone model was constructed with one isoprenyl unit, that is, 2,3-dimethoxy-5-methyl-6-isoprenyl-1,4-benzoquinone. Geometries were initially fully optimized using the same methods as for the test set of the present study. Subsequently, methoxy dihedral angles ($C_1C_2OC_{Me}$ for 2-methoxy and $C_4C_3OC_{Me}$ for 3-methoxy) were imposed as indicated by experimental studies, while the rest of the geometry was relaxed again, separately for the neutral and anionic states. The 3-methoxy group was fixed at the crystallographic midrange values of −77° for UQ_A and + 88° for UQ_B,[147] whereas the 2-methoxy groups were positioned so that the constraints on ^{13}C isotropic hyperfine couplings from the HYSCORE studies[141,142] are satisfied, +155° for UQ_A and − 82° for UQ_B.[143]

The basis set extrapolated DLPNO-CCSD(T_0) results indicate that UQB has a greater electron affinity (1.721 eV) than UQA (1.571 eV), and hence the conformation of methoxy groups creates an intrinsic difference of 150 meV between the two quinones. Although explicit consideration of the protein

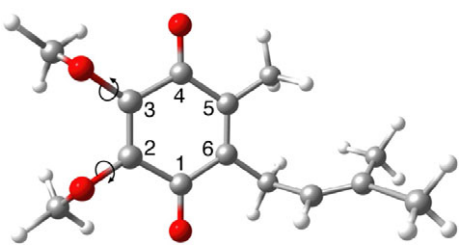

Figure 4. Ubiquinone model used in the calculation of the methoxy conformation effect. [Color figure can be viewed at wileyonlinelibrary.com]

environment (electrostatics and hydrogen-bonding) would be required for further refinement, we expect the results to be essentially exact within a few mV with respect to the intrinsic effect of the methoxy rotation difference. This is not only because the method performs very well in absolute terms for the test set of the present study, but also because in this particular application it would further benefit from error cancellation as only relative conformational effects for the same molecule are examined. DFT studies of the two ubiquinones assuming different methoxy conformations initially suggested a difference in electron affinities of merely 50 meV,[142] however subsequent studies that better combined crystallographic and ^{13}C HYSCORE information reported differences of more than 190 meV.[143] The present coupled cluster results correct the apparent overestimation by DFT (B3LYP), but otherwise confirm that the intrinsic difference in electron affinities created by the methoxy rotation is more than double that of the macroscopically observed potential.

Therefore, the conclusion regarding the ubiquinones of bacterial reaction centers appears solid: in contrast to the early classical electrostatic simulations,[137] our results support the notion[143] that the driving force for forward electron transfer from UQ_A to UQ_B is the combined result of two *opposing* contributions. The particular conformation of the methoxy groups, presumably imposed by steric constraints of the protein pocket, creates an electron affinity difference of 150 meV that overcomes the counteracting electrostatic effect of the protein environment, leading to an overall potential difference of approximately half this value. It remains to be examined in future studies why this compensating mechanism was evolutionarily selected, but we hypothesize it may be part of a broader regulatory/protective mechanism that allows the system to balance forward and backward electron transfer, potentially in response to external stimuli such as light intensity or the concentration of the ubiquinone pool.

Conclusions

A test set of 10 quinones relevant to quinones encountered in biology as electron transfer components was used to evaluate a range of wave function and density functional theory methods for the prediction of electron affinities. The results of the present study suggest that very few methods can deliver a level of accuracy systematically better than 0.1 eV. Density functionals perform very well in comparison to correlated wave function methods given their comparatively low cost, but only the double hybrids can consistently deliver this level of accuracy. All implementations of coupled cluster theory require some form of inclusion of the effect of triples excitations to reach the desired accuracy of better than 0.1 eV. The most accurate method, yielding reference-quality results with a mean signed error of 0.02 eV, is a composite approach that utilizes canonical CCSD(T) with a small basis set and LPNO-based extrapolation of the correlation energy with a sequence of larger basis sets. Somewhat less accurate but still highly reliable are the LPNO-based pCCSD, which simulates the effect of the triples through its parametrization, and the DLPNO-CCSD(T_0) which has the significant advantage that it can be extended to very large systems. In all cases basis set extrapolation is crucial. The bt-PNO-EOM-CCSD approach could not achieve an accuracy as high as subtraction-based extrapolation schemes that incorporate a CCSD(T) component. With inclusion of triples the EOM-CC approach is expected to perform more competitively and benefit from its intrinsic advantages over the subtractive approach. MP2 and orbital-optimized OO-SCS-MP2 methods perform well, whereas SCS-MP2 proves to be problematic for the present test set. Conversely, these MP2 methods are less systematic than the coupled cluster alternatives and suffer from a wider spread of errors. In the DFT world, typical GGA, meta-GGA, hybrid and long-range corrected functionals lead to systematic overestimation of electron affinities. The best performing functional among these families is the Minnesota functional M06, the only one which can achieve a mean unsigned error of the order of 0.1 eV. However, the most accurate functionals for the prediction of electron affinities are the double hybrids, with B2PLYP matching the accuracy of extrapolated coupled cluster methods.

Overall, it is suggested that one of the three highlighted coupled cluster approaches is to be preferred, depending on the system size and cost balance, when systematic and consistent performance is required, or for benchmarking other methods. The applicability of linear scaling coupled cluster methods was demonstrated by studying how the distinct orientation of the 2-methoxy group affects the electron affinity of the ubiquinone electron carriers in bacterial reaction centers. It was concluded that the conformational differences of the methoxy groups between the primary and terminal ubiquinone favor forward electron transfer much more strongly (by 150 meV) than the experimentally deduced reduction potential difference (ca. 70 mV), strongly suggesting that protein electrostatics oppose the intrinsic electron affinity difference of the two quinones as part of a regulatory mechanism. We expect that the increasing cost-effectiveness of approximate coupled cluster approaches will lead to their more widespread use in practical applications, replacing less robust approaches both as standalone techniques and as components of multiscale approaches.

Acknowledgment

Support by the Max Planck Society is gratefully acknowledged.

Keywords: quinones · electron affinities · coupled cluster · DLPNO methods · bacterial reaction centers

How to cite this article: C. E. Schulz, A. K. Dutta, R. Izsák, D. A. Pantazis. *J. Comput. Chem.* **2018**, *39*, 2439–2451. DOI: 10.1002/jcc.25570

Additional Supporting Information may be found in the online version of this article.

[1] R. E. Blankenship, Molecular Mechanisms of Photosynthesis, 2nd ed., Wiley, Chichester, **2014**.

[2] F. Müh, C. Glöckner, J. Hellmich, A. Zouni, Biochim. Biophys. Acta Bioenerg. **2012**, 1817, 44.
[3] V. Krewald, M. Retegan, D. A. Pantazis, Top. Curr. Chem. **2016**, 371, 23.
[4] K. Brettel, W. Leibl, Biochim. Biophys. Acta Bioenerg. **2001**, 1507, 100.
[5] P. Jordan, P. Fromme, H. T. Witt, O. Klukas, W. Saenger, N. Krauß, Nature **2001**, 411, 909.
[6] J. Deisenhofer, H. Michel, EMBO J. **1989**, 8, 2149.
[7] G. Feher, J. P. Allen, M. Y. Okamura, D. C. Rees, Nature **1989**, 339, 111.
[8] M. Y. Okamura, R. A. Isaacson, G. Feher, Proc. Natl. Acad. Sci. USA **1975**, 72, 3491.
[9] A. Rodenberg, M. Orazietti, M. Mosberger, C. Bachmann, B. Probst, R. Alberto, P. Hamm, ChemPhysChem **2016**, 17, 1321.
[10] E. J. Son, J. H. Kim, K. Kim, C. B. Park, J. Mater. Chem. A **2016**, 4, 11179.
[11] S. Er, C. Suh, M. P. Marshak, A. Aspuru-Guzik, Chem. Sci. **2015**, 6, 885.
[12] S. D. Pineda Flores, G. C. Martin-Noble, R. L. Phillips, J. Schrier, J. Phys. Chem. C **2015**, 119, 21800.
[13] A. V. Marenich, J. Ho, M. L. Coote, C. J. Cramer, D. G. Truhlar, Phys. Chem. Chem. Phys. **2014**, 16, 15068.
[14] J. E. Bachman, L. A. Curtiss, R. S. Assary, J. Phys. Chem. A **2014**, 118, 8852.
[15] N. Gillet, B. Lévy, V. Moliner, I. Demachy, A. de la Lande, J. Comput. Chem. **2017**, 38, 1612.
[16] S. Kishi, K. Saito, Y. Kato, H. Ishikita, Photosynth. Res. **2017**, 134, 193.
[17] C. Frontana, Á. Vázquez-Mayagoitia, J. Garza, R. Vargas, I. González, J. Phys. Chem. A **2006**, 110, 9411.
[18] X.-Q. Zhu, C.-H. Wang, J. Org. Chem. **2010**, 75, 5037.
[19] A. H. Pakiari, S. Siahrostami, A. Mohajeri, J. Mol. Struct. (THEOCHEM) **2008**, 870, 10.
[20] M. Namazian, S. Siahrostami, M. L. Coote, J. Fluorine Chem. **2008**, 129, 222.
[21] M. T. Huynh, C. W. Anson, A. C. Cavell, S. S. Stahl, S. Hammes-Schiffer, J. Am. Chem. Soc. **2016**, 138, 15903.
[22] M. Namazian, M. L. Coote, J. Phys. Chem. A **2007**, 111, 7227.
[23] M. Namazian, S. Siahrostami, M. R. Noorbala, M. L. Coote, J. Mol. Struct. (THEOCHEM) **2006**, 759, 245.
[24] E. P. Nafikova, N. L. Asfandiarov, L. R. Kalimullina, Y. N. El'kin, Russ. Chem. Bull. **2014**, 63, 572.
[25] S. E. Boesch, A. K. Grafton, R. A. Wheeler, J. Phys. Chem. **1996**, 100, 10083.
[26] A. K. Grafton, R. A. Wheeler, J. Phys. Chem. A **1997**, 101, 7154.
[27] M. Nonella, Photosynth. Res. **1998**, 55, 253.
[28] J. F. Stanton, R. J. Bartlett, J. Chem. Phys. **1993**, 98, 7029.
[29] J. F. Stanton, J. Gauss, J. Chem. Phys. **1994**, 101, 8938.
[30] J. Simons, Annu. Rev. Phys. Chem. **2011**, 62, 107.
[31] M. Nooijen, R. J. Bartlett, J. Chem. Phys. **1995**, 102, 3629.
[32] D. G. Liakos, F. Neese, J. Chem. Theory Comput. **2015**, 11, 4054.
[33] F. Neese, A. Hansen, D. G. Liakos, J. Chem. Phys. **2009**, 131, 064103.
[34] F. Neese, F. Wennmohs, A. Hansen, J. Chem. Phys. **2009**, 130, 114108.
[35] A. Hansen, D. G. Liakos, F. Neese, J. Chem. Phys. **2011**, 135, 214102.
[36] C. Riplinger, F. Neese, J. Chem. Phys. **2013**, 138, 034106.
[37] M. Saitow, U. Becker, C. Riplinger, E. F. Valeev, F. Neese, J. Chem. Phys. **2017**, 146, 164105.
[38] L. M. J. Huntington, M. Nooijen, J. Chem. Phys. **2010**, 133, 184109.
[39] L. M. J. Huntington, A. Hansen, F. Neese, M. Nooijen, J. Chem. Phys. **2012**, 136, 064101.
[40] S. Grimme, J. Chem. Phys. **2003**, 118, 9095.
[41] L. Kong, F. A. Bischoff, E. F. Valeev, Chem. Rev. **2012**, 112, 75.
[42] F. Neese, T. Schwabe, S. Kossmann, B. Schirmer, S. Grimme, J. Chem. Theory Comput. **2009**, 5, 3060.
[43] T. Schwabe, S. Grimme, Acc. Chem. Res. **2008**, 41, 569.
[44] Y. Zhao, D. G. Truhlar, Acc. Chem. Res. **2008**, 41, 157.
[45] S. Chowdhury, T. Heinis, E. P. Grimsrud, P. Kebarle, J. Phys. Chem. **1986**, 90, 2747.
[46] T. Heinis, S. Chowdhury, S. L. Scott, P. Kebarle, J. Am. Chem. Soc. **1988**, 110, 400.
[47] O. Burghaus, M. Plato, M. Rohrer, K. Moebius, F. MacMillan, W. Lubitz, J. Phys. Chem. **1993**, 97, 7639.
[48] E. K. Fukuda, R. T. McIver, J. Am. Chem. Soc. **1985**, 107, 2291.
[49] P. Kebarle, S. Chowdhury, Chem. Rev. **1987**, 87, 513.
[50] J. Tao, J. P. Perdew, V. N. Staroverov, G. E. Scuseria, Phys. Rev. Lett. **2003**, 91, 146401.
[51] F. Neese, WIREs Comput. Mol. Sci. **2012**, 2, 73.
[52] J. Zheng, X. Xu, D. G. Truhlar, Theor. Chem. Acc. **2011**, 128, 295.
[53] F. Weigend, R. Ahlrichs, Phys. Chem. Chem. Phys. **2005**, 7, 3297.
[54] F. Weigend, Phys. Chem. Chem. Phys. **2006**, 8, 1057.
[55] F. Neese, E. F. Valeev, J. Chem. Theory Comput. **2011**, 7, 33.
[56] D. Kats, F. R. Manby, J. Chem. Phys. **2013**, 139, 021102.
[57] D. Kats, J. Chem. Phys. **2014**, 141, 061101.
[58] D. Kats, D. Kreplin, H.-J. Werner, F. R. Manby, J. Chem. Phys. **2015**, 142, 064111.
[59] V. Rishi, A. Perera, M. Nooijen, R. J. Bartlett, J. Chem. Phys. **2017**, 146, 144104.
[60] D. G. Liakos, F. Neese, J. Phys. Chem. A **2012**, 116, 4801.
[61] D. Z. Goodson, J. Chem. Phys. **2002**, 116, 6948.
[62] F. Weigend, A. Köhn, C. Hättig, J. Chem. Phys. **2002**, 116, 3175.
[63] A. K. Dutta, F. Neese, R. Izsák, J. Chem. Phys. **2016**, 145, 034102.
[64] A. K. Dutta, F. Neese, R. Izsák, J. Chem. Phys. **2016**, 144, 034102.
[65] F. Neese, F. Wennmohs, A. Hansen, U. Becker, Chem. Phys. **2009**, 356, 98.
[66] R. Izsák, F. Neese, J. Chem. Phys. **2011**, 135, 144105.
[67] K. A. Peterson, T. B. Adler, H.-J. Werner, J. Chem. Phys. **2008**, 128, 084102.
[68] K. E. Yousaf, K. A. Peterson, J. Chem. Phys. **2008**, 129, 184108.
[69] J. P. Perdew, K. Burke, M. Ernzerhof, Phys. Rev. Lett. **1996**, 77, 3865.
[70] A. D. Becke, J. Chem. Phys. **1993**, 98, 5648.
[71] C. Lee, W. Yang, R. G. Parr, Phys. Rev. B **1988**, 37, 785.
[72] C. Adamo, V. Barone, J. Chem. Phys. **1999**, 110, 6158.
[73] Y. Zhao, D. G. Truhlar, Theor. Chem. Acc. **2008**, 120, 215.
[74] Y.-S. Lin, G.-D. Li, S.-P. Mao, J.-D. Chai, J. Chem. Theory Comput. **2013**, 9, 263.
[75] T. Yanai, D. P. Tew, N. C. Handy, Chem. Phys. Lett. **2004**, 393, 51.
[76] L. Goerigk, S. Grimme, J. Chem. Theory Comput. **2010**, 7, 291.
[77] S. Grimme, J. Chem. Phys. **2006**, 124, 034108.
[78] S. Kozuch, J. M. L. Martin, Phys. Chem. Chem. Phys. **2011**, 13, 20104.
[79] S. Kozuch, J. M. L. Martin, J. Comput. Chem. **2013**, 34, 2327.
[80] M. Piris, Int. J. Quantum Chem. **2006**, 106, 1093.
[81] M. Piris, X. Lopez, F. Ruiperez, J. M. Matxain, J. M. Ugalde, J. Chem. Phys. **2011**, 134, 164102.
[82] K. Pernal, K. J. Giesbertz, Top. Curr. Chem. **2016**, 368, 125.
[83] E. N. Zarkadoula, S. Sharma, J. K. Dewhurst, E. K. U. Gross, N. N. Lathiotakis, Phys. Rev. A **2012**, 85, 032504.
[84] M. Piris, J. M. Matxain, X. Lopez, J. M. Ugalde, J. Chem. Phys. **2012**, 136, 174116.
[85] A. W. Rutherford, A. Osyczka, F. Rappaport, FEBS Lett. **2012**, 586, 603.
[86] Y. Kato, R. Nagao, T. Noguchi, Proc. Natl. Acad. Sci. USA **2016**, 113, 620.
[87] K. Saito, A. W. Rutherford, H. Ishikita, Proc. Natl. Acad. Sci. USA **2013**, 110, 954.
[88] A. Krieger, A. W. Rutherford, G. N. Johnson, Biochim. Biophys. Acta Bioenerg. **1995**, 1229, 193.
[89] H. Ishikita, E.-W. Knapp, J. Am. Chem. Soc. **2005**, 127, 14714.
[90] H. Ishikita, K. Hasegawa, T. Noguchi, Biochemistry **2011**, 50, 5436.
[91] K. Hasegawa, T. Noguchi, Photosynth. Res. **2014**, 120, 113.
[92] K. Ido, C. M. Gross, F. Guerrero, A. Sedoud, T.-L. Lai, K. Ifuku, W. A. Rutherford, A. Krieger-Liszkay, J. Photochem. Photobiol. B **2011**, 104, 154.
[93] H. Bao, C. Zhang, Y. Ren, J. Zhao, Biochim. Biophys. Acta Bioenerg. **2010**, 1797, 339.
[94] R. Ashizawa, T. Noguchi, Phys. Chem. Chem. Phys. **2014**, 16, 11864.
[95] T.-J. Lin, P. J. O'Malley, J. Phys. Chem. B **2011**, 115, 4227.
[96] B. Rabenstein, G. M. Ullmann, E.-W. Knapp, Biochemistry **2000**, 39, 10487.
[97] F. Müh, A. Zouni, Photosynth. Res. **2013**, 116, 295.
[98] T. Shibamoto, Y. Kato, R. Nagao, T. Yamazaki, T. Tomo, T. Watanabe, FEBS Lett. **2010**, 584, 1526.
[99] C. Fufezan, C. M. Gross, M. Sjödin, A. W. Rutherford, A. Krieger-Liszkay, D. Kirilovsky, J. Biol. Chem. **2007**, 282, 12492.
[100] K. Brinkert, S. De Causmaecker, A. Krieger-Liszkay, A. Fantuzzi, A. W. Rutherford, Proc. Natl. Acad. Sci. USA **2016**, 113, 12144–12149.
[101] S. I. Allakhverdiev, T. Tsuchiya, K. Watabe, A. Kojima, D. A. Los, T. Tomo, V. V. Klimov, M. Mimuro, Proc. Natl. Acad. Sci. USA **2011**, 108, 8054.

[102] T. Cardona, A. Sedoud, N. Cox, A. W. Rutherford, Biochim. Biophys. Acta Bioenerg. **2012**, 1817, 26.
[103] A. Derks, K. Schaven, D. Bruce, Biochim. Biophys. Acta Bioenerg. **2015**, 1847, 468.
[104] M. Schreiber, M. R. Silva-Junior, S. P. A. Sauer, W. Thiel, J. Chem. Phys. **2008**, 128, 134110.
[105] J. R. Gour, P. Piecuch, M. Włoch, J. Chem. Phys. **2005**, 123, 134113.
[106] M. Musiał, S. A. Kucharski, R. J. Bartlett, J. Chem. Theory Comput. **2011**, 7, 3088.
[107] A. K. Dutta, T. Sengupta, N. Vaval, S. Pal, Int. J. Quantum Chem. **2015**, 115, 753.
[108] K. B. Bravaya, E. Epifanovsky, A. I. Krylov, J. Phys. Chem. Lett. **2012**, 3, 2726.
[109] K. B. Bravaya, O. Kostko, S. Dolgikh, A. Landau, M. Ahmed, A. I. Krylov, J. Phys. Chem. A **2010**, 114, 12305.
[110] A. A. Golubeva, A. I. Krylov, Phys. Chem. Chem. Phys. **2009**, 11, 1303.
[111] Y. Guo, C. Riplinger, U. Becker, D. G. Liakos, Y. Minenkov, L. Cavallo, F. Neese, J. Chem. Phys. **2018**, 148, 011101.
[112] J. C. Rienstra-Kiracofe, G. S. Tschumper, H. F. Schaefer, S. Nandi, G. B. Ellison, Chem. Rev. **2002**, 102, 231.
[113] L. A. Curtiss, P. C. Redfern, K. Raghavachari, J. A. Pople, J. Chem. Phys. **1998**, 109, 42.
[114] J. M. Galbraith, H. F. Schaefer, III., J. Chem. Phys. **1996**, 105, 862.
[115] N. Rösch, S. B. Trickey, J. Chem. Phys. **1997**, 106, 8940.
[116] A. A. Jarȩcki, E. R. Davidson, Chem. Phys. Lett. **1999**, 300, 44.
[117] H. B. Shore, J. H. Rose, E. Zaremba, Phys. Rev. B **1977**, 15, 2858.
[118] K. Schwarz, Chem. Phys. Lett. **1978**, 57, 605.
[119] K. Schwarz, J. Phys. B At. Mol. **1978**, 11, 1339.
[120] F. Jensen, J. Chem. Theory Comput. **2010**, 6, 2726.
[121] J. Simons, J. Phys. Chem. A **2008**, 112, 6401.
[122] D. Lee, F. Furche, K. Burke, J. Phys. Chem. Lett. **2010**, 1, 2124.
[123] M. Isegawa, F. Neese, D. A. Pantazis, J. Chem. Theory Comput. **2016**, 12, 2272.
[124] H. S. Yu, X. He, S. L. Li, D. G. Truhlar, Chem. Sci. **2016**, 7, 5032.
[125] L. Gallandi, N. Marom, P. Rinke, T. Körzdörfer, J. Chem. Theory Comput. **2016**, 12, 605.
[126] Y.-Y. Chuang, S.-M. Chen, J. Comput. Chem. **2011**, 32, 1671.
[127] A. Karton, J. M. L. Martin, J. Chem. Phys. **2011**, 135, 144119.
[128] R. Peverati, M. Head-Gordon, J. Chem. Phys. **2013**, 139, 024110.
[129] J. C. Sancho-García, A. J. Pérez-Jiménez, M. Savarese, E. Brémond, C. Adamo, J. Phys. Chem. A **2016**, 120, 1756.
[130] B. Chan, L. Goerigk, L. Radom, J. Comput. Chem. **2016**, 37, 183.
[131] W. M. C. Sameera, D. A. Pantazis, J. Chem. Theory Comput. **2012**, 8, 2630.
[132] T. Vikramaditya, S.-T. Lin, J. Comput. Chem. **2017**, 38, 1844.
[133] C. A. Wraight, Front. Biosci. **2004**, 9, 309.
[134] E. Takahashi, T. A. Wells, C. A. Wraight, Biochemistry **2001**, 40, 1020.
[135] L. J. Mancino, D. P. Dean, R. E. Blankenship, Biochim. Biophys. Acta Bioenerg. **1984**, 764, 46.
[136] D. Kleinfeld, M. Y. Okamura, G. Feher, Biochim. Biophys. Acta Bioenerg. **1984**, 766, 126.
[137] E. G. Alexov, M. R. Gunner, Biochemistry **1999**, 38, 8253.
[138] J.-R. Burie, C. Boullais, M. Nonella, C. Mioskowski, E. Nabedryk, J. Breton, J. Phys. Chem. B **1997**, 101, 6607.
[139] M. Nonella, J. Phys. Chem. B **1998**, 102, 4217.
[140] R. C. Prince, P. L. Dutton, M. J. Bruce, FEBS Lett. **1983**, 160, 273.
[141] A. T. Taguchi, A. J. Mattis, P. J. O'Malley, S. A. Dikanov, C. A. Wraight, Biochemistry **2013**, 52, 7164.
[142] A. T. Taguchi, P. J. O'Malley, C. A. Wraight, S. A. Dikanov, Biochemistry **2013**, 52, 4648.
[143] W. B. de Almeida, A. T. Taguchi, S. A. Dikanov, C. A. Wraight, P. J. O'Malley, J. Phys. Chem. Lett. **2014**, 5, 2506.
[144] W. B. de Almeida, P. J. O'Malley, Comput. Theor. Chem. **2015**, 1069, 11.
[145] A. Remy, R. B. Boers, T. Egorova-Zachernyuk, P. Gast, J. Lugtenburg, K. Gerwert, Eur. J. Biochem. **2003**, 270, 3603.
[146] C. A. Wraight, A. S. Vakkasoglu, Y. Poluektov, A. J. Mattis, D. Nihan, B. H. Lipshutz, Biochim. Biophys. Acta Bioenerg. **2008**, 1777, 631.
[147] C. A. Wraight, M. R. Gunner, In The Purple Phototrophic Bacteria; C. N. Hunter, F. Daldal, M. C. Thurnauer, J. T. Beatty, Eds., Springer Netherlands, Dordrecht, **2009**, p. 379.

Received: 21 April 2018
Revised: 6 August 2018
Accepted: 7 August 2018
Published online on 3 October 2018